# Fabrication and Characterization of the Ti-6Al-4V/Mg Scaffold

**S. M. Kalantari[a,*], H. Arabi[a], SH. Mirdamadi[a], S. A. Mirsalehi[a]**

[a,] *Department of Metallurgy and Materials Engineering, Iran University of Science and Technology, Narmak, Tehran, Iran.*

**ARTICLE INFO**

*Article history:*

Received 09 Dec 2014
Accepted 26 Feb 2015
Available online 30 June 2015

*Keywords:*

Ti-6Al-4V
Scaffold
Mg
Powder metallurgy
SBF

**ABSTRACT**

In this research, Ti–6Al–4V scaffolds were fabricated by powder metallurgical space holder technique. The magnesium (Mg) powder was evaporated and a skeleton of Ti-6Al-4V alloy was produced. For this purpose,Ti-6Al-4V and Mg powders mixture was compacted in a steel die by applying the uniaxial pressure of 500 MPa before sintering the green product in a sealed quartz tube at 900 °C for 2 hours. Employing Archimedes' principle and an Image Tool software, the total and open volume percent of porosities within the scaffolds were found to be in the range of 46-64% and 41-47%, respectively. Bioactivity properties of the scaffolds were investigated in a simulated body fluid (SBF). Scanning electron microscopy (SEM) and energy dispersive spectroscopy (EDS) were used for studying the specimens' surfaces after immersing for 28 days. The results showed that the amounts of calcium (Ca) and phosphor(P) deposited into the porous areas were more than that onthe smooth surfaces due to the presence of the Mg particles within the pores which provoked formation of the apatite layers.Changing in the pH values of the SBF during 18 days of immersion revealed a gradual improvement in pH level due to releasing $OH^-$.Atomic absorption spectroscopy (AAS) indicated that by increasing the Mg content of scaffolds, Ca concentration of SBF decreased, which is an indication of apatite formation on the scaffold.Results of SBF bioactivity examinationsexhibited that the scaffold with 60 vol.%of Mg has the best ability to induce apatite nucleation.

## 1. Introduction

Although a great progress has been madein orthopedic biomaterials, fixation of implants is still a crucial problem. Mismatch of Young's moduleof the biomaterials and the surrounding bone has been known as a main reason for implant loosening, following the stress shielding of the bone[1-7]. One solution to solve this problem in medical applications has been the development of materials that exhibit substantial surface or high total bulk porosity [3]. Poor mechanical properties of porous ceramic and polymeric biomaterials led researchers to focus on porous metals, based on orthopedic metallic materials, due to their superior fatigue and fracture resistance

Corresponding author:
*E-mail address:* kalantary.mohammad@gmail.com (Seyed Mohammad Kalantari).

characteristics, which are required for load-bearing applications[3]. Recently, titanium (Ti) and its alloys have been widely used as metallic biomaterials due to their excellent mechanical properties, wonderful biocompatibility, and good corrosion resistance [8-12]. Furthermore, Ti and its alloys are not ferromagnetic and do not cause harm to the patient in magnetic resonance imaging (MRI) units [13]. The most known Ti alloys, e.g.Ti-6Al-4V, are considered as having excellent tensile strength and pitting corrosion resistance [14].

One method to enhance osseointegration of titanium scaffold is the use of bioactive materials to provide the necessary bioactivity to the titanium with a porous network to facilitate osteoconduction [13]. Magnesium is a good candidate due to its excellent bioactivity. Mg has a density of 1.74 g/cm$^3$ , similar to that of natural bone [15, 16]. An adult human has about 30 g magnesium in his body, most of whichexistsin muscle and bone. Dietary magnesium deficiency has been identified as a risk factor for osteoporosis[16]. In addition, magnesium strongly binds to phosphates and through its control of hydroxyapatite (HA) (calcium phosphate) formation, influences the mineralization of the bony tissue [17].

There are two serious consequences of the corrosion process of Mg implants [18, 19]. The first is the formation of hydrogen gas bubbles which appear within one week after surgery and can be easily treated by drawing off the gas using a subcutaneous needle [19]. However, it is reported [18] that hydrogen ($H_2$) has the properties of anti-oxidation, anticancer, and anti-inflammatory due to reduction ofreactive free radicals. An article published in 2007 [20] has suggested that a hydrogen evolution rate of 0.01 ml/cm$^2$/day can be tolerated by the human body. Thus, it is reasonable to believe that hydrogen gas is not a serious problem. Another undesirable consequence of the Mg and its alloys degradation is rising in the pH value [18]. According to Nan et al. [18], the pH value had a great effect on the enzymatic activities of superoxide dismutase, peroxidase, and catalase in cells. The high pH value might lead to reduction in theactivity of these enzymes in cells [18].

Adding Mg to titanium by powder metallurgy technique could be a good idea to make it more bioactive and alsobiocompatible. In other words, in this study we have examined the effect of addition of bioactive material (Mg powder) to the Ti-6Al-4V scaffold. The idea behind choosing Mg as a space holder was that the addition of this material into the Ti-6Al-4V structure will provide a bioactive surface on theTi-6Al-4V scaffold, andthebioactive surface can improvethe formation of apatite nucleation on this scaffold. Thus, the apatite nucleation can be filled by osteoblast cells in in-vivo culture. Therefore, the remained Mg could play an important role in enhancing of scaffoldbioactivity. This process will enhance the osteointegration of scaffold with bone tissues. In this research Ti–6Al–4V alloy scaffolds with different amounts of Mg (30, 45, and 60 vol.%) powder were produced by powder metallurgy technique. The pore characteristics of the scaffolds (e.g.pore shape, size, and interconnectivity) were examined using scanning electron microscopy (SEM). The effect of the amount of Mg on bioactivity was determined by immersing samples in SBF and atomic absorption spectroscopy (AAS) was used to measurethe amount of Ca in the solution.

## 2. Experimental

### 2. 1. Preparing materials

Residual spring-like chips from machining process of Ti6Al4V bars were used as starting material. In order to determine the exact chemical composition of the as-received chips, quantometer analysis was applied on raw Ti-6Al-4V bar (Table 1). A similar chemical composition which agreed with the specification for Ti-6Al-4V powders was used for coating surgical and medical implants (ASTM F1580-01) [21].

Since the spring-like chips filled up most of the vial volume, preventing balls to move effectively in the milling process, they were manually crushed in a mortar prior to milling to obtain small pieces with a length of less than 1 cm. (Figure 1)

Planetary ball milling machine (Retsch PM400 type) under protective atmosphere of Ar (99.998% pure) was used to crush chips to

**Table 1.** Mean chemical composition of Ti-6Al-4V bar (wt.%)

| Element | Ti | Al | V | Cu | Mo | Sn | Si | Fe | Zr | Mn | C |
|---|---|---|---|---|---|---|---|---|---|---|---|
| wt.% | 88.04 | 6.33 | 4.99 | 0.01 | 0.02 | 0.00 | 0.00 | 0.48 | 0.00 | 0.01 | 0.77 |
| ASTM F1580-01 | Balance | 5.5-6.75 | 3.5-4.5 | 0.1 | - | 0.1 | - | 0.3 | - | - | 0.8 |

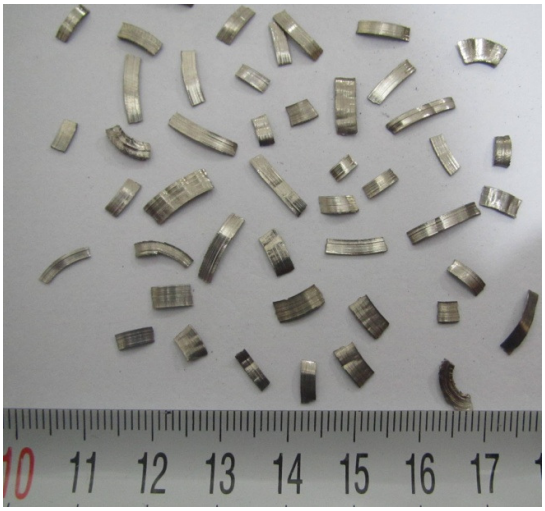


**Fig. 1.** Light micrograph of crushed chips before ball milling

much smaller pieces. The powder was ground in a tungsten carbide closed vial. The powder to ball mass ratio was about 1:10 and the rotation speed was maintained at 250 rpm. The milling operation was performed for 6 hours in such a way that the rotary machine was on for 20 min and then 10 min off for cooling. Ethanol was added to the vials to act as a coolant and to prevent excessive heat generation during ball milling. The crystal structure of the as-milled powder was characterized by means of X-ray diffraction (Philips X'PERT MPD) using filtered Cu-Kα radiation (k= 0.1542 nm).

### 2. 2. Composite production

Ti-6Al-4V and magnesium (Merck >99% pure) powders were sieved to obtain a powder range of 37–90μm for the base alloy and 90–180μm for Mg powder. Then various amounts of Mg powders (i.e.30%, 45% , and 60% Mg by volume fraction) were mixed with the alloy powder in an agate mortar using 5 wt.% polyvinyl alcohol (PVA) solution (5 wt.% PVA + 95% water) as the binder prior to compaction. PVA solution was required for the uniform coating of the coarse Mg particles with fine Ti-6Al-4V powders. Mixing time was determined as 30 min to assure a homogeneous distribution of the powders. Then the mixtures were uniaxially pressed undera pressure of 500 MPa in a steel die using a hydraulic press. The heat treatment process consisted of two steps, i.e. at 450 °C for 2 h to allow debinding of PVA and then 900 °C for 2 h for sintering. Argon flow rate was kept at a minimum adequate to provide a positive internal pressure inside the furnace to avoid possible leakage of air into the furnace. To reduce evaporation of Mg, the samples were placed in a quartz tube as shown in Figure 2.

### 2. 3. Pore characterization

Porosity contents of the Ti-6Al-4V/Mg scaffolds were determined via Archimedes' principle. The pore morphology and interconnectivity were observed using scanning electron microscopy (SEM, TESCAN VEGA//XMU). Some of the characteristics (e. g. size distribution, and roundness) were evaluated by image analyzer attached to an optical microscope and suitable analyzing software (e. g. Image Tool). For the image

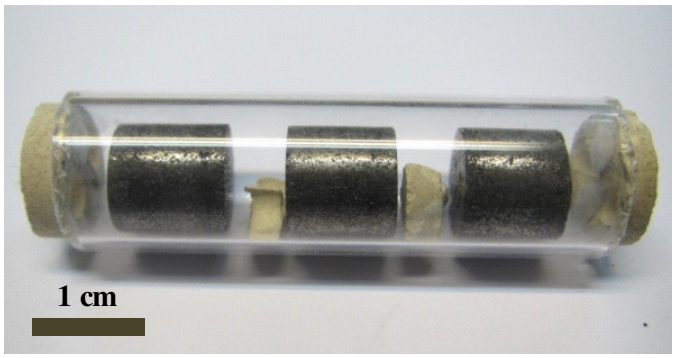


**Fig. 2.** Samples in a quartz tube in order to reduce Mg evaporation

**Table 2.** Chemical composition of the simulated body fluid (SBF) compared to the human blood plasma [22]

| | $Na^+$ | $K^+$ | $Mg^{2+}$ | $Ca^{2+}$ | $Cl^-$ | $HCO_3^-$ | $HPO_4^{2-}$ | $SO_4^{2-}$ |
|---|---|---|---|---|---|---|---|---|
| Blood plasma | 142.0 | 3.6-5.5 | 1.0 | 2.1-2.6 | 95.0-107.0 | 27.0 | 0.65-1.45 | 1.0 |
| SBF | 142.0 | 5.0 | 1.0 | 2.5 | 126.0 | 10.0 | 1.0 | 1.0 |

analysis, the sectioned parts were prepared by a sequence of conventional metallographic steps.

### 2. 4. Soaking in the simulated body fluid (SBF)

Before soaking the samples in SBF, their surfaces were polished with 600# grit silica papers and washed ultrasonically in acetone, alcohol and deionized water for 15 min. The sintered compacts were then immersed in SBF for up to 4 weeks to access its bioactivity. SBF wasprepared according to the Kokubo procedure. In this method, the reagent grade NaCl, KCl, $NaHCO_3$, $MgSO_4.12H_2O$, $CaCl_2$, and $KH_2PO_4$are dissolved into distilled water and buffered at pH = 7.4 with tri-hydroxymethylaminomethane (TRIS) and HCl at 37 ºC [22]. The ion concentration of the SBF is shown in Table 2.

The volumes (Vs; ml) for the immersion liquid were calculated based on the formula: $V_s=10 /S_a$ where $S_a$ ($cm^2$) was the surface area of each samples.

#### 2. 4. 1. Characterization of surface morphology

The specimens were taken out ofthe SBF after 28 days. Changes in the surface structureof the specimens were observed after immersing them in SBF for a certain time. These surfaces were characterized by scanning electron microscopy (SEM TESCAN VEGA//XMU) with energy dispersive spectroscopy (EDS) analysis.

#### 2. 4. 2. Measurement of calcium concentrations and pH

Changes in the concentrations of the calcium element in the SBF due to the immersion of the specimens were determined by atomic absorption spectroscopy (AAS GBC-Avanta ∑) technique after 2,9,18 and 28 days. Changes in the pH value of the fluid were also measured during 18 days. The SBF, in which the specimens for surface examination were immersed, was refreshed every two days. However, the SBF used for measuring pH and calcium concentration was not refreshed throughout the whole observation process.

## 3. Results and Discussion

### 3. 1. X-ray diffraction

The result of X-ray diffraction of the ball-milled alloy powder is presented in Figure 3.

The XRD spectrum reveals that the ball-milledpowder was mainly Ti6Al4V. No considerable change in the position of peaks was observed after ball milling, sothat all diffracted peaksare related to Ti-6Al-4V. Additionally, neither oxides nor nitrides were detected although titanium is a very reactive element and prone to form various oxides and nitrides such as TiO, $TiO_2$, $Ti_2O_3$, $Ti_3O_5$, TiN, etc. when it is in contact with oxygen, water vapor, air, and nitrogen gas. When the steel container and the steel ball were used for production of the powder, Fe contamination can be produced [23], while the use of a

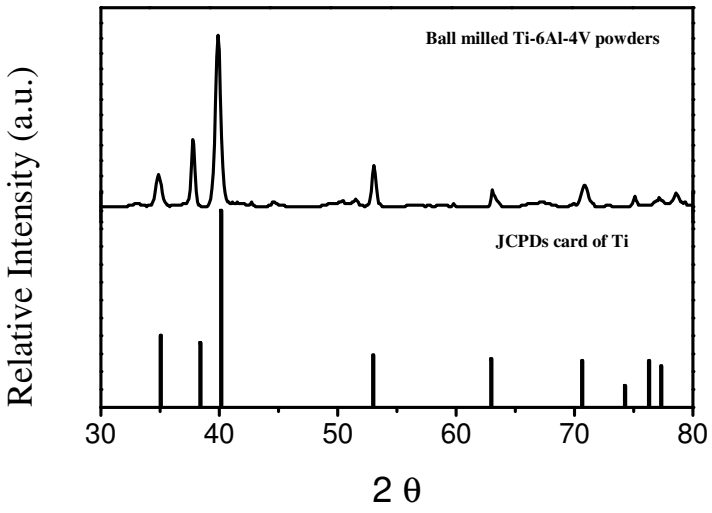


**Fig. 3.** The results of X-ray analysis for the prepared Ti-6Al-4V powders, together with the JCPDs card for Ti

**Table 3.** Pore characterizations extracted from software Image Tool and use of Archimedes' principle

| Sample | Total porosity (%) | Open porosity (%) | Roundness (%) |
|---|---|---|---|
| Ti6Al4V/30Mg | 46 | 41 | 25 |
| Ti6Al4V/45Mg | 53 | 43 | 22 |
| Ti6Al4V/60Mg | 64 | 47 | 28 |

tungsten carbide vial introduces no such contamination. This phenomenon can be attributed to higher friction coefficient of tungsten carbide compared to that of the steel balls.

### 3. 2. Characterization of porosity and pores

The results of the image analysis for specimens are summarized in Table 3.

The open porosity is expressed as a percentage of the interconnected pore space in total amount of porosity within the scaffolds. Image analysis indicated that total porosity and open porosity tend to increase from 46% and 41% to 64%, and 47%, respectively, with increasing the amount of magnesium. In fact, two types of pores remained after sintering. One was the small pores having several micrometers mean diametersinherited from the space among Ti6Al4V particles after compaction while the large pores were generated after the partial evaporation of magnesium. The pore size and shape were a function of the size and shape of the prime powders used. Typical pore morphologies of the scaffolds surfaces having different amounts of magnesium are presented in Figure 4.

Distribution of large pores in various samples can be seen in Figure 4. Their shapes are irregular and have different sizes due to the irregular shape and inconsistent sizes of the Mg particles. As the total porosity of the compacts increased, the average roundness of the pores also increased mainly due to the inter-connection of macro-pores at higher porosity levels which was found to be 28% for the sample with64% porosity. It should be noted that compacts with porosities morethan 20 vol.% are considered as promising samples for biomedical applications since it has been reported[24]that the optimal porosity of implant materials for ingrowths of new-bone tissues is in the range of 20–50 vol.%. The pore size distributions of the scaffolds are shown in Figure 5.

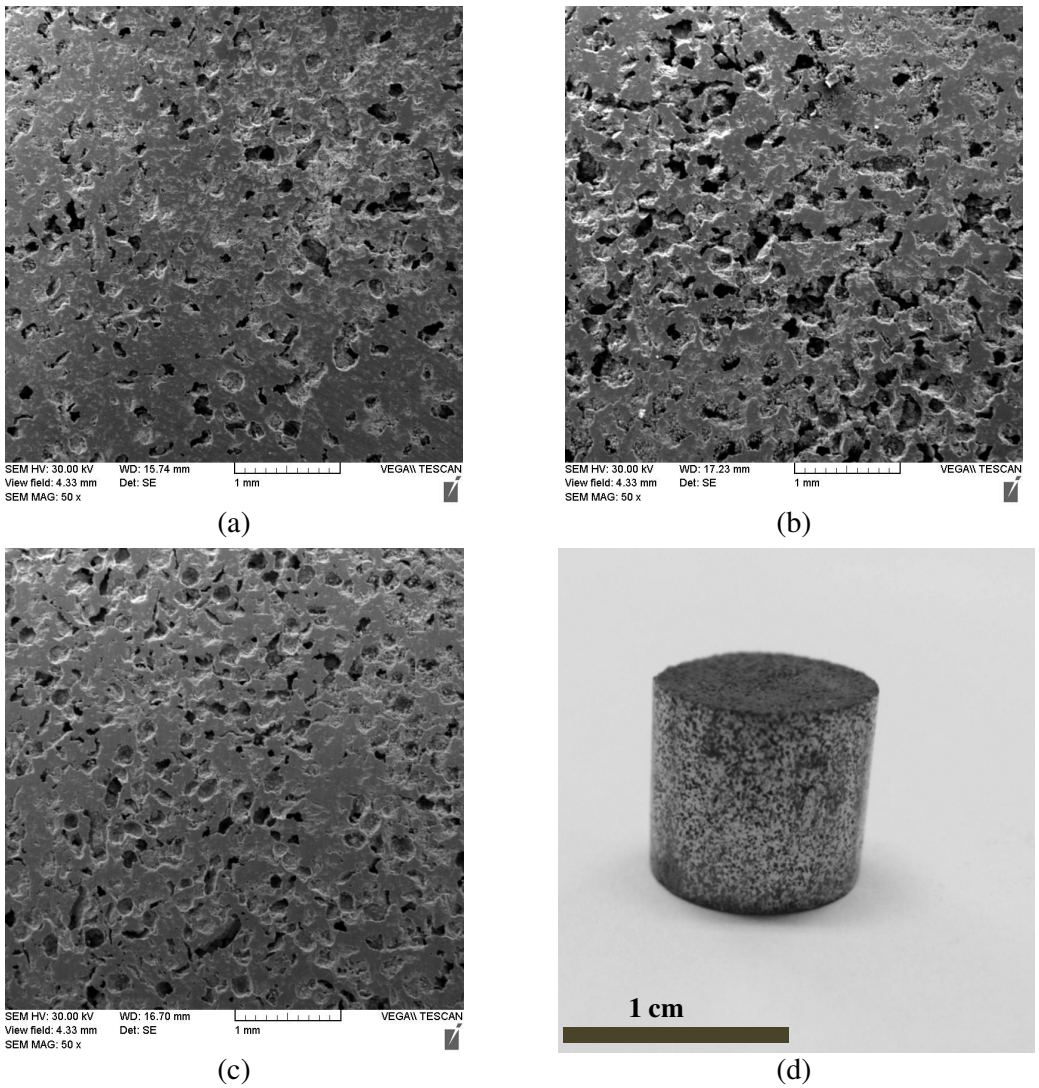


**Fig. 4.** SEM micrograph of pore morphology in: (a) Ti-6Al-4V/30vol.%Mg, (b) Ti-6Al-4V/45 vol.%Mg, and (c) Ti-6Al-4V/60 vol.% Mg. A typical macro-photo of the Ti-6Al-4V/Mg scaffold can be seen in (d)

The data presented in Figure 5 show that the pore size distributions are mainly in the range of 20-60 µm, and higher ranges were obtained in the samples with higher magnesium content. This phenomenon can be explained by considering the area of interconnected sites among the Mg granules. As these areas decreased, the initial content of Mg decreased and caused a decrease in the pore size. However, according to Bobyn et al. [25] and Itala et al.[26], the sizes of the pores generated due to sintering and partial evaporation of Mg are large enough for the consistent ingrowth of new bone within the porous space.

### 3. 3. SBF bioactivity

#### 3. 3. 1. SEM andEDS analysis

Typical micrographsof the specimens'surfaces with 30 and 60 vol.%of Mg after immersing in the SBF for 28 days are shown in Figure6. The SEM micrographs in this figure show a thin layer of Ca and P deposited on the surfaces.

After 28 days of immersion, the surfaces of thesesamples were analyzed by EDS and the results are presented in Figure 7. These spectrographs (Figure 7) show that by

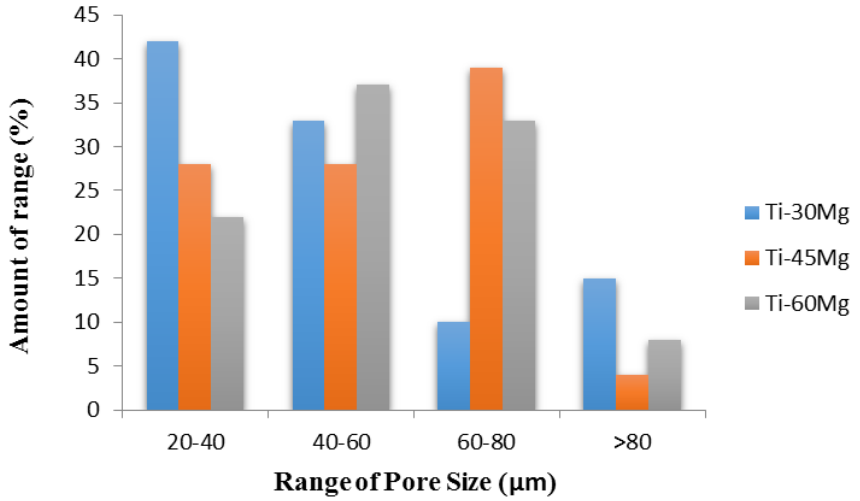


**Fig. 5.** Pore size distributions for the porous Ti6Al4V scaffolds produced having various initial Mg contents of 30, 45, and 60 vol.%

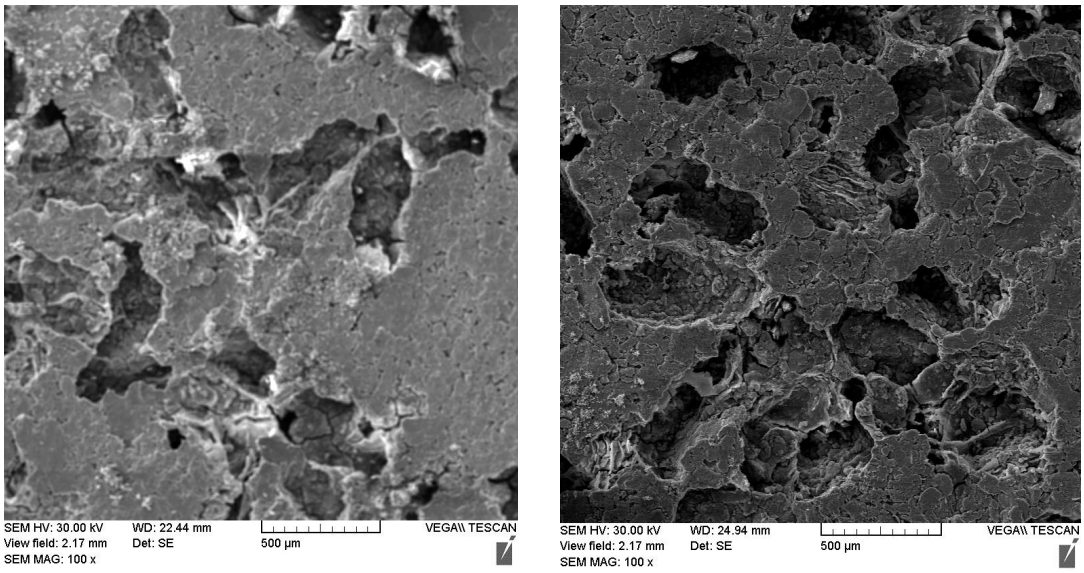


(a) (b)

**Fig. 6.** SEM micrographs of the scaffolds surfaces with (a) 30 and (b) 60 vol.% Mg after immersion in the SBF for 28 days

increasing the Mg content, the quantity of deposited Ca and P increased.

Typical distribution of calcium and phosphorus on the surface of one of the samples is shown in Figure 8. The amount of Ca and P deposited into the porous areas ismore than those deposited on smooth surfaces which resulted inan increase in biocompatibility property of the pores. It is worth mentioning that the primary cause of more Ca and P depositions in pores surfaces can be attributed to the presence of more Mg which caused the formation of a large number of porositiesdue to its partial evaporation during sintering.

### 3. 3. 2. pH value measurement

The changes occurred in the pH values of the

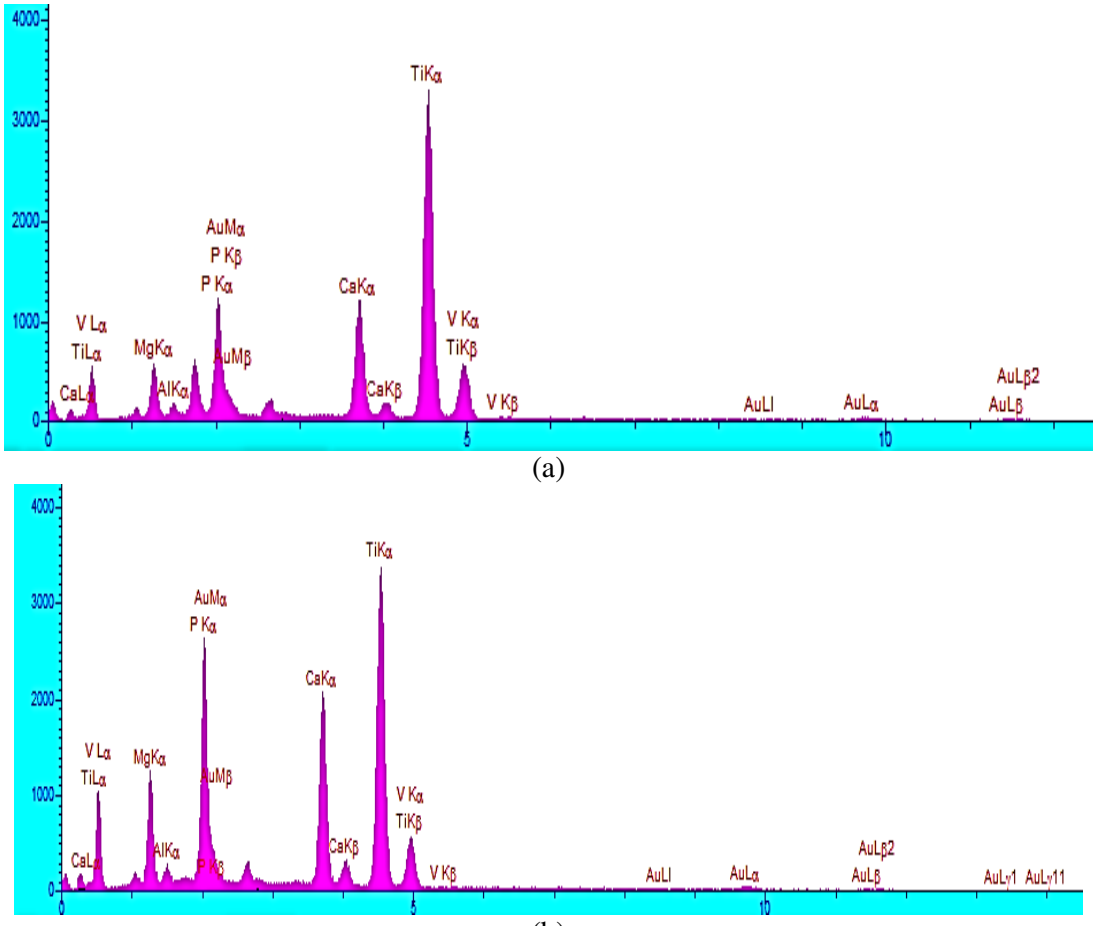


**Fig. 7.** EDS analysis of the scaffolds surfaces having (a) 30 and (b) 60 vol.% Mg after immersion in the SBF for 28 days

SBF, as a function of immersion time, are given in Figure 9. According to Figure 9, at first the pH values increased sharply due to the immersion of the scaffold in SBF and the sudden release of theMg ions. After 10 days, decreasing the amount of Mg leads to the slight stabilizationof the pH level.The pH values after 18 days of immersion were 8.76, 8.96, and 9.06 for the specimenswith 30, 45, and 60 vol.%of Mg, respectively. Corrosion of Mg in an aqueous physiological environment can be expressed by the following equations. The primary anodic reaction is expressed by the partial reaction presented in equation (1); at the same time, the reduction of protons is expressed by the partial reaction occurring on the cathode and can be presented by equation (2).

Anodic reaction: $Mg \rightarrow Mg^{2+} + 2e^{-}$ [1]

Cathodic reaction: $2H_2O + 2e^{-} \rightarrow 2OH^{-} + H_2$ [2]

Along with the progress of corrosion reaction, the pH of the solution near the Mg surface can be increased with the accumulation of $OH^{-}$, resulting in the precipitation of the $Mg(OH)_2$on the surface. This is due to the decrease in the solubility of $Mg(OH)_2$ with the increasing of the $OH^{-}$ concentration. It has been reported[19] thatthe accumulated $Mg(OH)_2$ layer on the Mg surface can act as a barrier against dissolution by preventing mass diffusion between the magnesium substrate and the solution. Thissuggests that the accumulated $Mg(OH)_2$ layer on the scaffold surface retarded the $Mg^{2+}$ release after near 12 days. Recently, Robinson et al. [27] reported the novel antibacterial

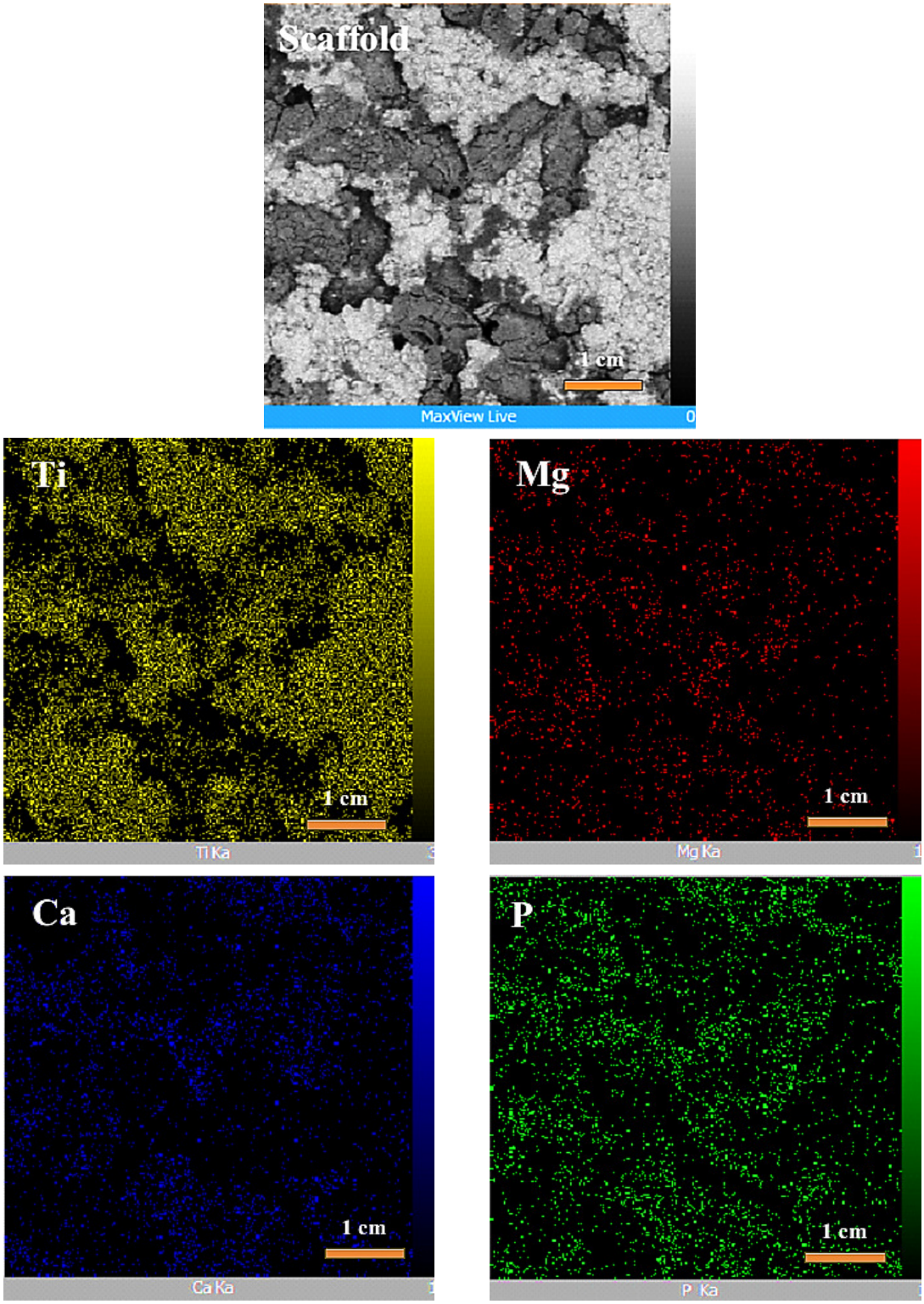


**Fig. 8.** SEM image and element mapping of scaffold with 60 vol.%of Mg after immersion into the SBF for 28 days duration. Magnification 500×

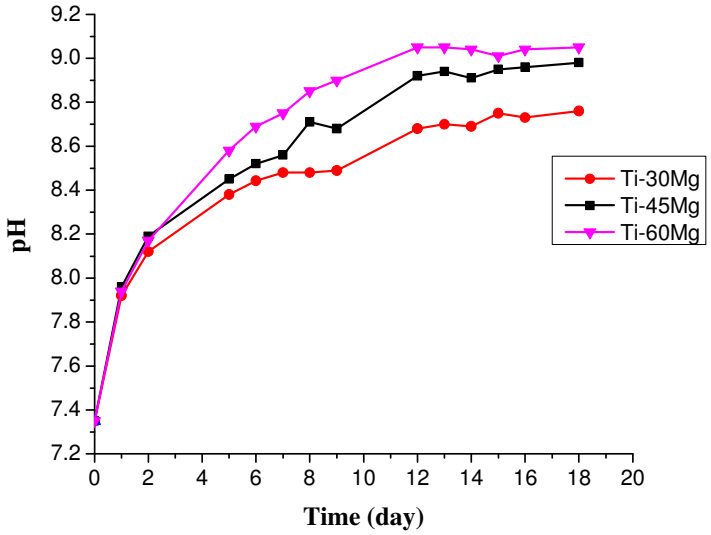


**Fig. 9.** Changes in pH value of the SBF as a function of immersion time

properties of the Mg metal against Escherichia coli, Pseudomonas aeruginosa and Staphylococcus aureus. In addition, Nan et al.[18] have stated that the pH value has a great effect on the enzymatic activities of superoxide dismutase, peroxidase, and catalase in cells. Therefore, the high pH values might lead to reduction in the activity of these enzymes in cells. However, as reported in reference [2] such extensive changes in pH would not be expected in vivo due to the fact that corrosion products can be easily evacuated from the implantation site by lymphatic circulatory systems and the buffering action of the tissue fluid.

### 3. 3. 3. Calcium concentration

The calcium concentration as a function of immersion time is shown in Figure 10.

This figure indicates that byincreasing the immersion time in SBF, calcium concentration of this solutiongraduallydecreases. The nucleation and growth of the apatite on the porous surfaces consume calcium and phosphorus in the solution resulting incalcium reduction in the SBF.

The pH values increased with increasing the mass fraction of magnesium. This increase can easily reach two pH units which leads to a 10–100-fold decrease of HA solubility and, accordingly, a very large acceleration of apatite nucleation according to Bohner et al. [28]. Kuwahara et al. [29] who declared that the corrosion products on the surface of Mg immersed in Hank's solution might be amorphous and complicated in their structure. They reported the formation of a compound such as $(Ca_{0.86}Mg_{0.14})_{10}(PO_4)_6(OH)_2$. Considering the similar ion concentrations in the SBF used in this study to those in Hank's solution[29], some amorphous phosphates containing magnesium/calcium might have been formed in this study. According to Jonasova et al. [30], the solution with ions such as $PO_4^{-3}$,$Ca^{+2}$etc, HA is likely to nucleate and grow on the magnesium surface due to the supersaturated condition at high pH. Moreover, when the $Mg^{2+}$ ions are dissolved into the solution, phosphates containing Mg/Ca form and tightly attach to the matrix. In general, the reaction among$H_n PO_4^{(3-n)-}$,$Ca^{+2}$and $Mg^{+2}$could be described primarily as:

H_n PO_4^((3-n)-)+Ca^(+2)+Mg^(+2)+OH^-→Mg_x Ca_y (PO_4 )_z [3]

Taking the excess $OH^-$ into consideration, some researchers reported [31] that complicated compounds [represented by $Mg_xCa_y(PO_4)_z(OH)$] might be deposited on the

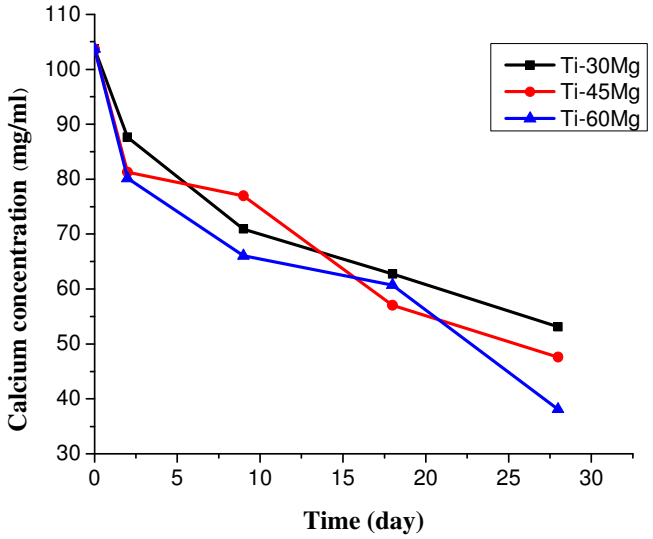


**Fig. 10.** Changes in calcium concentrations as a function of immersion time

surface. Xu et al. [32] also reported that the corrosion layer containing such magnesium-substituted calcium phosphate compounds on Mg can promote osteoinductivity and osteoconductivity, predicting good biocompatibility of magnesium.

## 4. Conclusions

Ti-6Al-4V scaffolds having various amounts of Mg elements in composition were successfully fabricated by powder metallurgy technique. Partial evaporation of magnesium during sintering caused the formation of evenly distributed pores within the scaffold. The following conclusions are drawn:

1- Total and open porosities of the scaffolds were within the ranges of 46-64 vol.% and 41-47 vol.%, respectively. The degree of roundness of the pores was within the range of 22-28%.

2- Two ranges of the pores were obtained; one was in the range of 50-100μm and the other was several micrometers long. Therefore, a bimodal distributing pore size was obtained which makes the fabricated scaffolds suitable for application as biomaterials.

3- After immersion for 28 days in simulation body fluid, calcium and phosphorus precipitated on the interior surfaces but more on pores surfaces. This shows the ability of the scaffold to induce apatite nucleation and growth on these surfaces.

4- The pH values rose with increasing the mass fraction of magnesium. This increase can easily lead to decrease of the HA solubility and, accordingly, a very large acceleration of apatite nucleation.

5- Deposition of calcium and phosphorus in the porous areas was more than that onthe smoother areas of the scaffold surfaces. This was attributed to the higherpresence of Mg in the porous areas resulting inmore partial evaporation of Mg in these areas.

6- Results of the SBF bioactivity examination showed that the scaffold having 60 vol.%of Mg has the best ability to induce apatite nucleation and the most deposition of Ca and P.

## Acknowledgement

We are pleased to acknowledge that this work was financially supported by Mr. GhasemKalantari.

## References

1. Y. F. Zheng, X. N. Gu, F. Witte, Biodegradable metals, Materials Science and Engineering: R:

Reports, 77, 2014, pp. 1-34.
2. A. Pietak, P. Mahoney, G. J. Dias, M. P. Staiger, Bone-like matrix formation on magnesium and magnesium alloys, Journal of Materials Science: Materials in Medicine, 19, 2008, pp. 407-415.
3. G. Ryan, A. Pandit, D. P. Apatsidis, Fabrication methods of porous metals for use in orthopaedic applications, Biomaterials, 27, 2006, pp. 2651-2670.
4. Y. Chen, B. Feng, Y. Zhu, J. Weng, J. Wang, X. Lu, Fabrication of porous titanium implants with biomechanical compatibility, Materials Letters, 63, 2009, pp. 2659-2661.
5. S. W. Kim, H. D. Jung, M.-H. Kang, H.-E. Kim, Y.-H. Koh, Y. Estrin, Fabrication of porous titanium scaffold with controlled porous structure and net-shape using magnesium as spacer, Materials Science and Engineering: C, 33, 2013, pp. 2808-2815.
6. M. Niinomi, Mechanical properties of biomedical titanium alloys, Materials Science and Engineering: A, 243, 1998, pp. 231-236.
7. B. Arifvianto, J. Zhou, Fabrication of Metallic Biomedical Scaffolds with the Space Holder Method: A Review, Materials, 7, 2014, pp. 3588-3622.
8. G. Ryan, P. McGarry, A. Pandit, D. Apatsidis, Analysis of the mechanical behavior of a titanium scaffold with a repeating unit-cell substructure, Journal of Biomedical Materials Research Part B: Applied Biomaterials, 90, 2009, pp. 894-906.
9. Y. Oshida, Bioscience and bioengineering of titanium materials, Elsevier, 2010.
10. S. N. Dezfuli, S. Sadrnezhaad, M. Shokrgozar, S. Bonakdar, Fabrication of biocompatible titanium scaffolds using space holder technique, Journal of Materials Science: Materials in Medicine, 23, 2012, pp. 2483-2488.
11. J. Li, J. De Wijn, C. Van Blitterswijk, K. De Groot, Porous Ti6Al4V scaffolds directly fabricated by 3D fibre deposition technique: effect of nozzle diameter, Journal of Materials Science: Materials in Medicine, 16, 2005, pp. 1159-1163.
12. N. Ayda, M. Alam, M. Ravindranath, Corrosion in titanium dental implants: literature review, The Journal of Indian prosthodonic society, 5, 2005, pp. 126-131.
13. K. Alvarez, H. Nakajima, Metallic scaffolds for bone regeneration, Materials, 2, 2009, pp. 790-832.
14. H. Hermawan, Introduction to Metallic Biomaterials, in: Biodegradable Metals, Springer, 2012, pp. 1-11.
15. W. F. Ng, K. Y. Chiu, F. T. Cheng, Effect of pH on the in vitro corrosion rate of magnesium degradable implant material, Materials Science and Engineering: C, 30, 2010, pp. 898-903.
16. R. Zeng, W. Dietzel, F. Witte, N. Hort, C. Blawert, Progress and challenge for magnesium alloys as biomaterials, Advanced Engineering Materials, 10, 2008, B3-B14.
17. H. Zreiqat, C. Howlett, A. Zannettino, P. Evans, G. Schulze-Tanzil, C. Knabe, M. Shakibaei, Mechanisms of magnesium-stimulated adhesion of osteoblastic cells to commonly used orthopaedic implants, Journal of biomedical materials research, 62, 2002, pp. 175-184.
18. M. Nan, C. Yangmei, Y. Bangcheng, Magnesium metal—A potential biomaterial with antibone cancer properties, Journal of Biomedical Materials Research Part A, (2013).
19. A. Yamamoto, S. Hiromoto, Effect of inorganic salts, amino acids and proteins on the degradation of pure magnesium in vitro, Materials Science and Engineering: C, 29, 2009, pp. 1559-1568.
20. G. Song, Control of biodegradation of biocompatable magnesium alloys, Corrosion Science, 49, 2007, pp. 1696-1701.
21. A. F1580-01, Standard Specification for Titanium and Titanium-6 Aluminum-4 Vanadium Alloy Powders for Coatings of Surgical Implants
22. T. Kokubo, H. Takadama, How useful is SBF in predicting in vivo bone bioactivity Biomaterials, 27, 2006, pp. 2907-2915.
23. A. Mahboubi Soufiani, M. Enayati, F. Karimzadeh, Fabrication and characterization of nanostructured Ti6Al4V powder from machining scraps, Advanced Powder Technology, 21, 2010, pp. 336-340.
24. I.-H. Oh, N. Nomura, N. Masahashi, S. Hanada, Mechanical properties of porous titanium compacts prepared by powder sintering, Scripta Materialia, 49, 2003, pp. 1197-1202.
25. J. Bobyn, J. Miller, Features of biologically fixed devices, orthopaedic basic science. Am Acad Orthop Surg, 10, 1994, pp. 613-616.
26. A. I. Itälä, H. O. Ylänen, C. Ekholm, K. H. Karlsson, H. T. Aro, Pore diameter of more than 100 μm is not requisite for bone ingrowth in rabbits, Journal of biomedical materials research, 58, 2001, pp. 679-683.
27. D. A. Robinson, R. W. Griffith, D. Shechtman, R. B. Evans, M. G. Conzemius, In vitro antibacterial properties of magnesium metal against Escherichia coli, Pseudomonas

aeruginosa and Staphylococcus aureus, Acta biomaterialia, 6, 2010, pp. 1869-1877.
28. M. Bohner, J. Lemaitre, Can bioactivity be tested in vitro with SBF solution Biomaterials, 30, 2009, pp. 2175-2179.
29. H. Kuwahara, Y. Al-Abdullat, N. Mazaki, S. Tsutsumi, T. Aizawa, Precipitation of magnesium apatite on pure magnesium surface during immersing in Hank's solution, Materials Transactions(Japan), 42, 2001, pp. 1317-1321.
30. L. Jonášová, F. A. Müller, A. Helebrant, J. Strnad, P. Greil, Biomimetic apatite formation on chemically treated titanium, Biomaterials, 25, 2004, pp. 1187-1194.
31. S. Ibasco, F. Tamimi, R. Meszaros, D. L. Nihouannen, S. Vengallatore, E. Harvey, J.E. Barralet, Magnesium-sputtered titanium for the formation of bioactive coatings, Acta biomaterialia, 5, 2009, pp. 2338-2347.
32. L. Xu, G. Yu, E. Zhang, F. Pan, K. Yang, In vivo corrosion behavior of Mg-Mn-Zn alloy for bone implant application, Journal of Biomedical Materials Research Part A, 83, 2007, pp. 703-711.